Published online 29 April 2019

Nucleic Acids Research, 2019, Vol. 47, No. 11 ***5465–5479***
doi: 10.1093/nar/gkz247

NAR Breakthrough Article

Site-specific replacement of phosphorothioate with alkyl phosphonate linkages enhances the therapeutic profile of gapmer ASOs by modulating interactions with cellular proteins

Michael T. Migawa, Wen Shen, W. Brad Wan, Guillermo Vasquez, Michael E. Oestergaard, Audrey Low, Cheryl L. De Hoyos, Ruchi Gupta, Susan Murray, Michael Tanowitz, Melanie Bell, Joshua G. Nichols, Hans Gaus, Xue-hai Liang, Eric E. Swayze, Stanley T. Crooke and Punit P. Seth*

Ionis Pharmaceuticals, 2855 Gazelle Court, Carlsbad, CA 92010, USA

Received February 14, 2019; Revised March 21, 2019; Editorial Decision March 22, 2019; Accepted April 02, 2019

ABSTRACT

Phosphorothioate-modified antisense oligonucleotides (PS-ASOs) interact with a host of plasma, cell-surface and intracellular proteins which govern their therapeutic properties. Given the importance of PS backbone for interaction with proteins, we systematically replaced anionic PS-linkages in toxic ASOs with charge-neutral alkylphosphonate linkages. Site-specific incorporation of alkyl phosphonates altered the RNaseH1 cleavage patterns but overall rates of cleavage and activity versus the on-target gene in cells and in mice were only minimally affected. However, replacing even one PS-linkage at position 2 or 3 from the 5′-side of the DNA-gap with alkylphosphonates reduced or eliminated toxicity of several hepatotoxic gapmer ASOs. The reduction in toxicity was accompanied by the absence of nucleolar mislocalization of paraspeckle protein P54nrb, ablation of P21 mRNA elevation and caspase activation in cells, and hepatotoxicity in mice. The generality of these observations was further demonstrated for several ASOs versus multiple gene targets. Our results add to the types of structural modifications that can be used in the gap-region to enhance ASO safety and provide insights into understanding the biochemistry of PS ASO protein interactions.

INTRODUCTION

Phosphorothioate-modified antisense oligonucleotides (PS-ASOs) interact with a host of plasma, cell-surface and intracellular proteins which govern their pharmacokinetic, pharmacological and toxicological properties (1,2). Within cells, PS ASOs interact with ∼60 cellular proteins such as P54nrb which have RNA-recognition motifs (RRMs) as well as chaperone proteins such as HSP90 which lack RNA- or DNA-binding domains and other proteins (3,4). ASO-binding proteins can affect ASO activity and subcellular distribution, causing them to localize to different sub-cellular foci, e.g., cytoplasmic sites such as endosomes, Golgi-related structure, P-bodies and stress granules, and the nucleus including the nucleolus and other nuclear sites such as paraspeckles (5,6).

We recently demonstrated a mechanism that explains the toxicities of the majority of toxic PS gapmer ASOs (7), including the three chemical classes most frequently used in gapmer therapeutics—2′-methoxyethyl RNA (MOE) (8), locked nucleic acid (LNA) (9,10) and constrained ethyl bridged nucleic acid (cEt) (11). Gapmer ASOs have a central gap-region of 7–12 phosphorothioate (PS) modified DNA flanked on either end with modifications which enhance nuclease stability and affinity for complementary RNA (8). Gapmer ASOs bind their targeted RNA in cells and the resulting RNA/DNA duplexes are substrates for RNaseH1, which selectively cleaves the RNA strand of the heteroduplex (12,13). Mammalian RNaseH1 is a ubiquitously expressed endonuclease which is comprised of three domains: catalytic, linker and hybrid-binding domain (HBD).

*To whom correspondence should be addressed. Tel: +1 760 603 2587; Email: pseth@ionisph.com

Our recent investigations revealed that toxic ASOs show enhanced binding to cellular proteins as compared to safe ASOs, and cause RNaseH1-dependent nucleolar mislocalization of paraspeckle proteins including P54nrb, nucleolar stress and fragmentation, upregulation of P21 mRNA and activation of caspase activity indicative of apoptosis (7). Introducing 2′-OMe RNA (OMe) at gap-position 2 from the 5′ wing-gap junction reduced global protein binding, and mitigated cytotoxicity in cells and hepatotoxicity in mice resulting in an improvement in therapeutic index (TI).

Given the importance of PS backbone for interaction with proteins (14–16), we systematically replaced anionic PS-linkages in toxic ASOs with charge-neutral methylphosphonate (MP) linkages (17). MPs have been known almost as long as the PS-modification but have only been used sparingly in the context of ASO drug-discovery (18). MPs do not support RNaseH1-mediated RNA cleavage near the site of incorporation into an ASO. MPs can be incorporated into nucleic acids using standard chemistry, but MP-modified oligonucleotides are more susceptible to strand cleavage under the basic conditions required to deprotect oligonucleotides after solid-phase synthesis. To address this limitation, we designed the methoxypropylphosphonate (MOP) linkage (Figure 1A), which has more steric bulk than MP but similar structural properties as the methoxyethyl group in MOE nucleosides, and examined its potential for enhancing the therapeutic profile of gapmer ASOs.

In this manuscript, we report the biophysical and biological evaluation of gapmer ASOs where one or more PS-linkages were replaced with alkylphosphonates. Site-specific incorporation of MOP altered the RNaseH1 cleavage patterns but overall rates of cleavage and activity versus the on-target gene in cells and in mice were only minimally affected. However, replacing even one PS-linkage at position 2 or 3 from the 5′-side of the DNA-gap with alkylphosphonates reduced or eliminated toxicity of several hepatotoxic gapmer ASOs. The reduction in toxicity was accompanied by the absence of nucleolar mislocalization of paraspeckle protein P54nrb, ablation of P21 mRNA elevation, and caspase activation in cells and hepatotoxicity in mice. The generality of these observations was further demonstrated for several ASOs versus multiple gene targets. Our results extend the generality of the mechanism of toxicity, add to the types of structural modifications that can be used in the gap-region to enhance therapeutic index and provide insights into understanding the biochemistry of PS ASO protein interactions.

MATERIALS AND METHODS

Synthesis of *N*,*N*,*N*',*N*'-tetraisopropyl-1-(3-methoxypropyl) phosphanediamine

Magnesium metal (4.18 g, 171 mmol) was suspended in dry THF (150 ml) in a dry round bottom flask (250 ml capacity) and was purged with dry nitrogen. 1-Bromo-3-methoxypropane (106 mmol, 12 ml) was added in portions via syringe over ∼20 min. The reaction was slightly exothermic and was immersed in a water bath (no ice) to control the temperature. The reaction was stirred for an additional 10 min after addition was complete. In a separate dry round bottom flask (1 L capacity), 1-chloro-*N*,*N*,*N*',*N*'-tetraisopropylphosphanediamine (93.8 mmol, 25 g) was suspended in dry Et_2O (300 ml), and the reaction was cooled in an ice bath (0°C) with stirring under nitrogen. The Grignard reagent (generated above) was transferred to the chlorophosphine suspension via cannula. The reaction was allowed to come to room temperature and was stirred for 1 h. The reaction was monitored by ^{31}P NMR. The reaction mixture was filtered through a plug of celite, and the solids were rinsed with Et_2O. The filtrates were pooled, and the solvent was removed on a rotary evaporator. The residue was suspended in dry acetonitrile (∼75 ml). The reaction mixture was transferred to a separatory funnel and was extracted with hexanes (∼250 ml). The hexanes layer was washed with acetonitrile (2 × 150 ml). The hexanes layer was collected and passed thru a plug of cotton to remove particulates and traces of water. The filtrate was concentrated a rotary evaporator and the residue was dried under high vacuum briefly to yield the phosphine reagent as an oil (27.10 g, 84%), which was used immediately for the next reaction. ^{31}P NMR (121 MHz, $CDCl_3$) δ = 47.70.

General method for the synthesis of mop phosphoramidites

The 5′-*O*-DMTr-protected nucleoside (1 equiv.) was dissolved in dry DMF (0.1 M) followed by addition of 1*H*-tetrazole (0.8 equiv.) and 1-methyl imidazole (0.44 equiv.). The MOP phosphorylation reagent from above (1.5 equiv.) was added and the reaction was allowed to stir at room temperature for 12–16 h under nitrogen. Upon completion the solvent was removed using a rotary evaporator (keep bath temperature under 35°C). The residue was diluted with EtOAc (100 ml) and transferred to a separatory funnel. The organic layer was washed with H_2O/brine (1:1, 200 ml) mixture, followed by H_2O/saturated aqueous $NaHCO_3$ (1:1, 2 × 200 ml), and finally with saturated NaCl (1 × 100 ml). The organics were pooled, dried over $MgSO_4$, filtered and concentrated. The residue was purified by silica gel chromatography to yield the desired phosphoramidite as a foam.

5′-*O*-(4,4′-Dimethoxytrityl)-3′-*O*-[3-methoxypropyl(di isopropylamino)phosphinyl]-2′-deoxy-(4-*N*-benzoyl)-adenosine (MOP-dA phosphoramidite). The protected nucleoside (15 g, 22.8 mmol) was converted to MOP-dA phosphoramidite (19.6 g, 82.9% yield). ^{31}P NMR (121 MHz, CDCl3-d) δ = 127.31, 126.19. Calcd for $C_{48}H_{57}N_6O_7P$, MW = 860.99; ESI-MS *m*/*z*: $[M\text{-}H]^-$, found 860.4.

5′-*O*-(4,4′-dimethoxytrityl)-3′-*O*-[3-methoxypropyl(di isopropylamino)phosphinyl]-2′-deoxy-(2-*N*-isobutyryl)-guanosine (MOP-dG phosphoramidite). The protected nucleoside (10 grams, 15.6 mmol) was converted to MOP-dG phosphoramidite (13.2 grams, 76% yield). ^{31}P NMR (121MHz, CDCl3-d) δ = 125.78, 125.10. Calcd. for $C_{45}H_{59}N_6O_8P$, MW = 842.96; ESI-MS m/z: $[M\text{-}H]^-$, found 842.4.

5′-*O*-(4,4′-Dimethoxytrityl)-3′-*O*-[3-methoxypropy l(diisopropylamino)phosphinyl]-2′-deoxy-(6-*N*-benzoyl-5-methyl)-cytidine (MOP-dC phosphoramidite). The protected nucleoside (11 g, 17.9 mmol) was converted to MOP-dC phosphoramidite (14.6 g, 84% yield). ^{31}P NMR

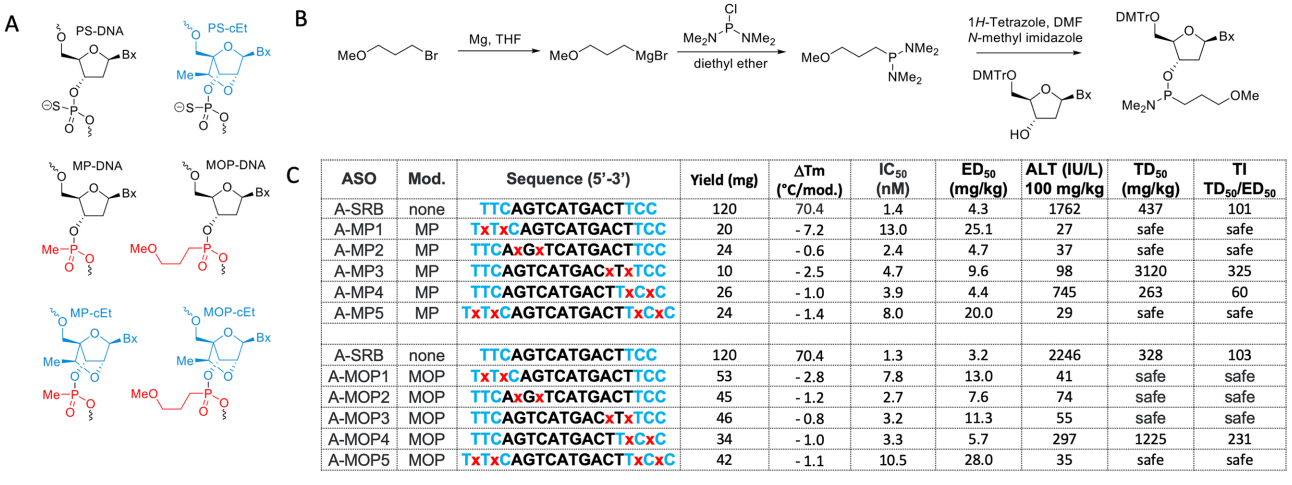

ASO	Mod.	Sequence (5'-3')	Yield (mg)	ΔTm (°C/mod.)	IC_{50} (nM)	ED_{50} (mg/kg)	ALT (IU/L) 100 mg/kg	TD_{50} (mg/kg)	TI TD_{50}/ED_{50}
A-SRB	none	TTCAGTCATGACTTCC	120	70.4	1.4	4.3	1762	437	101
A-MP1	MP	TxTxCAGTCATGACTTCC	20	-7.2	13.0	25.1	27	safe	safe
A-MP2	MP	TTCAxGxTCATGACTTCC	24	-0.6	2.4	4.7	37	safe	safe
A-MP3	MP	TTCAGTCATGACxTxTCC	10	-2.5	4.7	9.6	98	3120	325
A-MP4	MP	TTCAGTCATGACTTxCxC	26	-1.0	3.9	4.4	745	263	60
A-MP5	MP	TxTxCAGTCATGACTTxCxC	24	-1.4	8.0	20.0	29	safe	safe
A-SRB	none	TTCAGTCATGACTTCC	120	70.4	1.3	3.2	2246	328	103
A-MOP1	MOP	TxTxCAGTCATGACTTCC	53	-2.8	7.8	13.0	41	safe	safe
A-MOP2	MOP	TTCAxGxTCATGACTTCC	45	-1.2	2.7	7.6	74	safe	safe
A-MOP3	MOP	TTCAGTCATGACxTxTCC	46	-0.8	3.2	11.3	55	safe	safe
A-MOP4	MOP	TTCAGTCATGACTTxCxC	34	-1.0	3.3	5.7	297	1225	231
A-MOP5	MOP	TxTxCAGTCATGACTTxCxC	42	-1.1	10.5	28.0	35	safe	safe

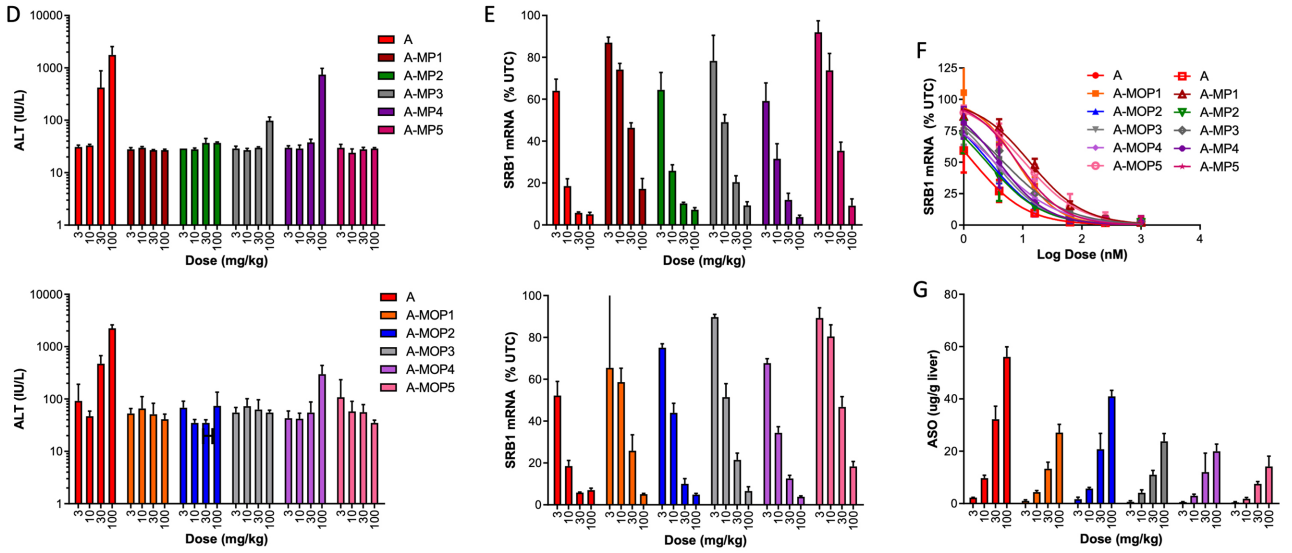

H

ASO	ED_{50} (mg/kg)	TD_{50} (mg/kg)	TI (TD_{50}/ED_{50})
A-SRB	2.5	148	59
A-MP2	4.5	safe	safe
A-MOP2	4.2	safe	safe

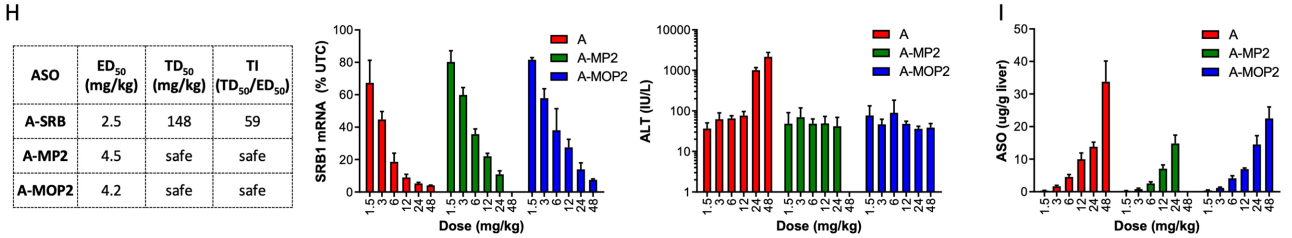

Figure 1. Replacing PS with neutral alkylphosphonate linkages near 5′-end of the DNA gap improves therapeutic profile of toxic gapmer ASOs. (**A**) Structures of MP and MOP-modified DNA and cEt nucleotides. (**B**) Synthesis of MOP-modified nucleoside phosphoramidites. (**C**) Sequence, ASO design (blue letters – cEt, black – PS DNA, red – MOP linkage), T_m versus complementary RNA, activity in primary mouse hepatocytes after ASO delivery by free uptake, potency for reducing SRB1 mRNA by 50% in mouse liver (ED_{50}), plasma ALT (IU/L) in mice 72 hours after injection of 100 mg/kg ASO, ASO dose (mg/kg) required to produce half-maximal elevations in plasma ALT (TD_{50}), Therapeutic index (TI) was calculated as the ratio of TD_{50} divided by the ED_{50}. ASOs were deemed safe if no elevation in plasma ALT were observed at the highest dose tested. (**D**) Plasma ALT (IU/L) levels following treatment with MP- or MOP-ASOs. (**E**) SRB1 mRNA reduction in liver in mice following treatment with MP- or MOP-ASOs. Balb-c mice were injected subcutaneously with 3, 10, 30 and 100 mg/kg of ASO and sacrificed 72 h after injection. Livers were harvested and changes in SRB1 mRNA relative to saline-treated control animals were quantified by qRT-PCR. (F) SRB1 mRNA reduction in primary mouse hepatocytes treated with MP- or MOP-ASOs by free uptake. (**G**) Liver accumulation of MOP-ASOs from dose-response experiment described in Figure 1E. ASO tissue levels were determined utilizing an HELISA assay. (**H**) Confirmation dose response to determine ED_{50} and plasma ALT (IU/L) levels for ASOs A, A-MP2 and A-MOP2. Balb-c mice were injected subcutaneously with 1.5, 3, 6, 12, 24 and 48 mg/kg of ASO and sacrificed 72 h after injection. Livers were harvested and changes in SRB1 mRNA relative to saline-treated control animals were quantified by qRT-PCR. (**I**) Liver accumulation (ug/g) for ASOs A, A-MP2 and A-MOP2 from confirmatory dose–response study as determined using HELISA. All errors are ±std.dev.

(121MHz, CDCl3-d) δ = 127.02. Calcd. for $C_{45}H_{61}N_4O_8P$, MW = 816.98; ESI-MS *m/z*: $[M-H]^-$, found 816.4.

5′-*O*-(4,4′-Dimethoxytrityl)-3′-*O*-[3-methoxypropyl(diisopropylamino)phosphinyl]-2′-deoxythymidine (MOP-dT phosphoramidite). The protected nucleoside (8.2 g, 15 mmol) was converted to MOP-dT phosphoramidite (9.25 g, 82% yield). ^{31}P NMR (121MHz, CDCl3-d) δ = 126.95. Calcd. for $C_{41}H_{54}N_3O_8P$, MW = 747.87; ESI-MS *m/z*: $[M-H]^-$, found 747.4.

(1*S*,3*R*,4*R*,6*S*,7*S*)-7-[3-Methoxypropyl(diisopropylamino)phosphinyl]-1-(4,4′-dimethoxytrityloxymethyl)-3-(6-*N*-Benzoyladenin-9-yl)-6-methyl-2,5-dioxa-bicyclo[2.2.1]heptane (MOP cEt A phosphoramidite). The protected nucleoside (10 g, 14.3 mmol) was converted to MOP cEt A phosphoramidite (11.1 g, 12.5 mmol, 87.6% yield). ^{31}P NMR (121 MHz, CDCl3-d) δ = 136.13, 129.87. Calcd. for $C_{50}H_{59}N_6O_8P$, MW = 903.03; ESI-MS *m/z*: $[M-H]^-$, found 903.4.

(1*S*,3*R*,4*R*,6*S*,7*S*)-7-[3-Methoxypropyl(diisopropylamino)phosphinyl]-1-(4,4′-dimethoxytrityloxymethyl)-3-(2-*N*-Isobutyrylguanin-9-yl)-6-methyl-2,5-dioxa-bicyclo[2.2.1]heptane (MOP cEt G phosphoramidite). The protected nucleoside (10 g, 14.7 mmol) was converted to MOP cEt G phosphoramidite (7.58 g, 8.6 mmol, 58.4% yield). ^{31}P NMR (121 MHz, CDCl3-d) δ = 135.40, 129.11. Calcd. for $C_{47}H_{61}N_6O_9P$, MW = 885.01; ESI-MS m/z: $[M-H]^-$, found 884.5.

(1*S*,3*R*,4*R*,6*S*,7*S*)-7-[3-methoxypropyl(diisopropylamino)phosphinyl]-1-(4,4′-dimethoxytrityloxymethyl)-3-(5-methyl-4-*N*-benzoylcytosin-1-yl)-6-methyl-2,5-dioxa-bicyclo[2.2.1]heptane (MOP cEt C phosphoramidite). The protected nucleoside (15 grams, 22.9 mmol) was converted to MOP cEt C phosphoramidite (13.9 grams, 71% yield). ^{31}P NMR (121MHz, CDCl3-d) δ = 135.85, 129.66. Calcd. for $C_{47}H_{63}N_4O_9P$, MW = 859.01; ESI-MS *m/z*: $[M–H]^-$, found 858.5.

(1*S*,3*R*,4*R*,6*S*,7*S*)-7-[3-Methoxypropyl(diisopropylamino)phosphinyl]-1-(4,4′-dimethoxytrityloxymethyl)-3-(thymin-1-yl)-6-methyl-2,5-dioxa-bicyclo[2.2.1]heptane (MOP cEt T phosphoramidite). The protected nucleoside (15 g, 25.6 mmol) was converted to MOP cEt T phosphoramidite (13.3 grams, 66% yield). ^{31}P NMR (121 MHz, CDCl3-d) δ = 135.85, 129.05. Calcd. for $C_{43}H_{56}N_3O_9P$, MW = 789.91; ESI-MS *m/z*: $[M–H]^-$, found 789.4.

Oligonucleotide synthesis and purification

Oligonucleotides were synthesized on a 40 μmol scale using Nittophase UnyLinker support (317 μmol/g) on an AKTA 10 Oligopilot. Fully protected nucleoside phosphoramidites were incorporated using standard solid-phase oligonucleotide synthesis, i.e. 15% dichloroacetic acid in toluene for deblocking, 1 M 4,5-dicyanoimidazole 0.1 M *N*-methylimidazole in acetonitrile as activator for amidite couplings, 20% acetic anhydride in THF and 10% 1-methylimidazole in THF/pyridine for capping and 0.1 M xanthane hydride in pyridine:acetonitrile 1:1 (v:v) for thiolation. MOP couplings were oxidized instead of thiolated using 20% *t*-BuOOH in ACN. Amidites were dissolved to 0.1 M in acetonitrile:toluene 1:1 (v:v) and incorporated using 6 min. coupling recycling time for DNA amidites and 10 min for all other amidites. At the end of the solid phase synthesis cyanoethyl protecting groups were removed by a 30 min treatment with 20% diethylamine in toluene. ASOs with a single MOP incorporation were deprotected and cleaved using conc. aq. ammonia at room temperature for 48 h. For ASOs with multiple MOP incorporations, the following mild deprotection conditions were used: Protected oligonucleotide on support (400 mg) was suspended in dry THF (5 ml) and stirred for 5 min in a glass pressure vial. Ethylenediamine (EDA, 5 ml) was added via syringe with stirring at room temperature. The reaction was heated 55°C with stirring (oil bath) for 15 min. The reaction was cooled in an ice bath, and was diluted with THF (5 ml). The reaction was centrifuged (300 rpm, 5 min), and the solvent was removed via pipette. The residue was washed with dry THF (2 × 5 ml). The pellet was suspended in 50% EtOH and the spent resin was removed by filtration. The filtrate was concentrated under reduced pressure. Oligonucleotides were purified by ion-exchange chromatography on a GE Akta Explorer 100 HPLC using aqueous buffers with 100 mM NH_4OAc and up to 2 M NaBr. The DMT group was removed on-column by treatment with 6% dichloroacetic acid in water. Pure fractions were desalted on a C18 reverse phase column, eluted in 50% acetonitrile in water (v:v) and lyophilized. Purity and mass of oligonucleotides was determined using ion-pair LCMS (Supplementary Figure S1).

T_m measurements

For the T_m experiments, ASO and RNA were mixed in 1:1 ratio (4 μM duplex) in a buffer containing 100 mM NaCl, 10 mM phosphate and 10 mM EDTA at pH 7. Oligos were hybridized with the complementary RNA strand by heating duplex to 85°C for 5 min and allowed to cool at room temperature. Thermal denaturation temperatures (T_m values) were measured in quartz cuvettes (pathlength 1.0 cm) on a Cary 100 ultraviolet (UV)/visible spectrophotometer equipped with a Peltier temperature controller. Absorbance at 260 nm was measured as a function of temperature using a temperature ramp of 0.5°C per min. T_m values were determined using the hyperchromicity method incorporated into the instrument software.

Cell culture and ASO treatment

HeLa, 3T3L1 and Hepa1-6 cells were grown at 37°C, 7.5% CO_2 in DMEM supplemented with 10% FBS and 1% penicillin/streptomycin. For transfection with PS-ASOs, cells at 70% confluency were transfected with ASOs at specified dose using Lipofectamine 2000 (Thermo Fisher Scientific) at a 4 μg/ml final concentration. For high-throughput electroporation of PS-ASOs for caspase 3/7 Glo assay or qRT-PCR, cells (20 000 cells/reaction) were mixed with PS-ASO at the specified final concentrations at a final volume of 100 μl and added to a BTX high throughput electroporation plate. The cells were then electroporated at 140 V for 3T3L1 cells respectively using an ECM 830 high throughput electroporation system.

Caspase activity assay

Caspase-Glo 3/7 Reagent was added directly to the cells at the volume equal to sample volume. Luminescence were recorded at 30 min by TECAN infinite M200. Background readings were determined from wells containing culture medium without cells and were subtracted from the control or assay readings. Relative caspase activity (%) was calculated as: 100 × luminescence reading of a treated sample/luminescence reading of an untreated control.

Animal experiments

Animal experiments were conducted in accordance with the American Association for the Accreditation of Laboratory Animal Care guidelines and were approved by the Animal Welfare Committee (Cold Spring Harbor Laboratory's Institutional Animal Care and Use Committee guidelines). Animals were housed in micro-isolator cages on a constant 12-h light–dark cycle with controlled temperature and humidity and were given access to food and water *ad libitum*. Animals were randomly grouped, and all animals were included in data analysis except those found dead. All experiments were done with $n = 3$ or 4 per dose group, except the single dose ALT screens at 150 mg/kg which were done with $n = 1$/group. 6–8-week-old Balb-C mice (Charles Rivers Laboratory) were treated with a single subcutaneous injection. Seventy two hours following treatment animals were sacrificed and blood and tissues were collected. For mice treated with the CXCl12 targeting ASOs, the groups for measuring ALT elevations were sacrificed at 72 h while the groups for mRNA evaluation were sacrificed at 24 h post injections, due to severe hepatoxicity observed at the 72 h timepoint for the parent ASO A-CXC. Blood was collected by cardiac puncture exsanguination with K_3-EDTA (SARSTEDT, Germany) and plasma transaminases were measured using a Beckman Coulter AU480 analyzer. Briefly, 50–100 mg of liver tissue was homogenized with an Omni Tissue Homogenizer (Omni International) in guanidinium thiocyanate with 8% beta mercaptoethanol, and total RNA was isolated using the PureLink Pro 96 Total RNA Purification Kit (Life Technologies, Carlsbad, CA, USA). qRT-PCR was performed in triplicate using the StepOne Real-Time PCR system and TaqMan primer probe sets with Express One-Step SuperMix qRT-PCR Kit (Life Technologies, Carlsbad, CA). Primers and probes for the PCR reactions were obtained either from ABI or Integrated DNA technologies (IDT). The sequences for the primers and probe used were as follows. Mouse SRB1: 5′-TGACA ACGACACCGTGTCCT-3′ for the forward primer, 5′-A TGCGACTTGTCAGGCTGG-3′ for the reverse primer, and 5′-CGTGGAGAACCGCAGCCTCCATT-3′ for the probe. Mouse CXCL12: 5′-CCAGAGCCAACGTCAAGC AT-3′ for the forward primer, 5′- CAGCCGTGCAAC AATCTGAA-3′ for the reverse primer, and 5′-TGAAA ATCCTCAACACTCCAAACTGTGCC-3′ for the probe. Mouse Hdac2: 5′-TGATGGTGTTGAGGAAGCTTTTT -3′ for the forward primer, 5′-TCCCTCAAGTCTCCTGT TCCA-3′ for the reverse primer, and 5′-ACAACAGAT CGCGTGATGACCGTCTC-3′ for the probe. Mouse Dynamin2: 5′-AGAGGAGACCGAGCGAAT-3′ for the forward primer, 5′-CATGGTTTGTGTTGATGTACGAC-3′ for the reverse primer, and 5′-CCTACATCAGGGAGC GAGAAGGGA-3′ for the probe. Mouse Fbo1a: 5′-GTC AAGACTACAACACACAGC-3′ for the forward primer, 5′-AAAACTATAAGGAGGGGTGAAGG-3′ for the reverse primer, and 5′-CTGAAGGACTTTTAAATGTAG CCTGCTCACTAA-3′ for the probe. Target RNA levels were normalized to the levels of total RNA measured by RiboGreen, RNA Quantitation Reagent (Molecular Probes). Dose response curves were plotted using GraphPad Prizm 5 software. Data was fitted using the log(inhibitor) versus response – Variable slope (four parameters) option. For ED_{50} (dose which reduces the targeted mRNA by 50% relative to saline treated animals) calculations, the bottom and top were fixed to 0 and 100 respectively. For TD_{50} (ASO dose which causes half-maximal ALT elevations) calculations, the bottom and top were fixed at 20 and 15000, which represent the lower and highest levels respectively, of plasma ALT elevations seen prior to death in mice. Therapeutic index was defined as the ratio of TD_{50} divided by the ED_{50}. ASOs were deemed safe if no elevation in plasma ALT were observed at the highest dose tested as the program was unable to fit a curve to calculate the TD_{50}.

RNA preparation and qRT-PCR analysis

Mouse liver punches were homogenized using Bio-Gen PRO200 Homogenizer (PRO Scientific). Total RNAs were isolated using TRIzol (Thermo Fisher Scientific) or RNeasy 96 Kits (Qiagen) according to protocols supplied by the manufacturers. TaqMan One-step qRT-PCR was performed using AgPath-ID™ One-Step RT-PCR Reagents (Thermo Fisher Scientific). Reverse transcription was performed at 45°C for 10 min, the reactions were then denatured at 95°C for 10 min, and forty cycles of PCR reactions were conducted at 95°C for 15 s and 60°C for 60 s within each cycle, using Applied Biosystems StepOnePlus Real-Time PCR system. Expression levels of target RNA were normalized to total RNA quantified using Quant-iT RiboGreen RNA Reagent (Thermo Fisher Scientific). qRT-PCR data was analyzed by StepOne Software v.2.2.2 (Applied Biosystems). Statistics analysis was performed using Prism, with *F*-test for curve comparison based on nonlinear regression (dose–response curves) for XY analyses, using equation 'log(agonist) versus normalized response–variable slope. The Y axis (relative mRNA level) was directly used as the normalized response.

Liver perfusion

Mice were anesthetized with an intraperitoneal injection of 0.1 ml per 10 g ketamine/xylazine. The inferior vena cava was catheterized and clamped. Liver was perfused with Hank's Balanced Salt Solution (Thermo Fisher) and mesenteric vessel was cut for drainage. Liver was subsequently perfused with collagenase (Roche). Following the perfusion, liver was removed and gently massaged through nylon mesh. Cells were washed in complete medium containing Williams' Medium E containing 10% fetal bovine serum, HEPES, GlutaMAX, and antibiotic/antimycotic (Thermo Fisher). The whole liver cell suspension was centrifuged at 50g. The resulting hepatocyte pellet was centrifuged in a

30% Percoll (GE Healthcare) gradient at 50g. A final wash was performed to remove residual percoll. Cells were resuspended in complete medium. Cell concentration and viability were determined on Countess II cell counter (Thermo Fisher).

ASO treatment of primary mouse hepatocytes via free uptake

Primary mouse hepatocytes were diluted to 100 000 cells/ml in room temperature complete medium before adding 100 μl of the cell suspension to the wells of a primaria coated 96-well culture plate (Corning). Immediately after plating the cells, 11 μl of 10× oligonucleotide in water was added to the appropriate wells. The culture plate was shaken for 30 s before incubating at 37°C and 5% CO_2 for 24 h. Cells were then washed with 100 μl PBS before being lysed in 40 μl GITC buffer for RNA isolation and analysis.

RNA isolation and quantitative PCR of primary mouse hepatocytes

RNA was extracted and purified with a glass fiber filter plate (Pall # 5072) and chiotropic salts. Messenger RNA expression levels were quantitated with quantitative reverse transcription PCR on the QuantStudio7 PCR Instrument (Applied Biosystems). Briefly, 10 μl RT-qPCR reactions containing 4 μl of RNA were run with Agpath-ID reagents (Applied Biosystems) and gene specific TaqMan primer probe sets (Integrated DNA Technologies) following the manufacturer's instructions. Total RNA levels, measured with Quant-iT Ribogreen Reagent (Thermo Fisher), were used to normalize the RT-qPCR data.

Immunofluorescent staining

Cells seeded on glass-bottom culture dishes (MatTek) were treated as described. After rinsing three times with 1× PBS, cells were fixed at room temperature with 4% formaldehyde for 30 min and permeabilized with 0.1% Triton X-100 in 1× PBS for 5 min. Fixed cells were then blocked in blocking buffer (1 mg/ml BSA in 1× PBS) at room temperature for 30 min and then incubated in blocking buffer with primary antibodies at room temperature for 2 h. After washing three times with washing buffer (0.1% Tween-20 in 1× PBS; 5 min per wash), cells were incubated in blocking buffer with secondary antibodies at room temperature for 1 h. Finally, cells were washed three times in washing buffer for 5 min each wash and mounted with Prolong Gold anti-fade reagent with DAPI (Molecular Probes). Confocal images were generated by confocal laser scanning microscopy using an FV1000 Fluoview (Olympus) and analyzed using Fluoview Ver. 2.0b Viewer (Olympus).

RNaseH1 cleavage assay

RNA substrate (5′-UAAUGUGAGAACAUGC-3′) was 5′-end labeled with P^{32} using T4 PNK, and gene-purified. 200 nM un-labelled and 1 nM labeled RNA substrate were mixed and annealed with 400 nM ASO in 20 μl hybridization buffer (20mM Tris pH 7.5; 50 mM NaCl; 2 mM $MgCl_2$; 0.2 mM TCEP; 2 U RNAseOUT), by heating at 90°C for 2 min, and gradually cooling at RT for 1 h. Next, 1 μl human RNase H1 protein (19) was added to the annealing mixture at 37°C, and incubated at 37°C for different times as indicated in figure legends. The enzymatic reaction was quenched by adding 20 μl of 8M Urea with loading dye, and heated at 90°C for 2 min, and chilled on ice. The samples were separated on 12% PAGE. The gel was dried, and image was visualized by autoradiography using PhosphorImager. The full length and cleaved products were quantified using ImageQuantTL software.

Protein-binding assay

Streptavidin magnetic beads (Millipore; 25 μl per reaction) were washed in binding buffer (1× PBS with 0.2% Tween-20) three times and incubated with 25 μM biotinylated capture PS-ASOs in 200 μl binding buffer at room temperature for 30 min. The beads were washed three times with binding buffer and incubated at 4°C for 2 h with 500 μg HeLa cell extract prepared in IP lysis buffer (Pierce). The beads were washed with the washing buffer (1× PBS with 0.2% Tween-20, with additional 100 mM NaCl) ten times and incubated with competitor non-biotinylated PS-ASOs at specified concentrations (0.33×, 1× and 3× of the concentration of the capture PS-ASO) for 5 min at room temperature with constant rotation. Supernatants were collected as eluted proteins. The proteins were separated on a 4–12% SDS-PAGE gel, and silver staining (SIGMA-ALDRICH) was performed to visualize the isolated PS-ASO-binding proteins.

Method to measure ASO tissue accumulation by HELISA

ASO tissue levels were determined utilizing an HELISA assay (20). 20 mg of tissue was homogenized in 500 μl of G2 buffer and digested with 5 units/ml of proteinase K overnight. A 25 μl aliquot of sample and capture probe was incubated at 65°C for 0.5 h in binding buffer while shaking, followed by incubation at 21°C for 1h. Samples were transferred to a streptavidin coated assay plate and incubated for 0.5 h at 21°C. After washing the plate two times, detected probe was added and incubated at 21°C for 1 h. Samples and a calibration curve spiked in tissue was read with a plate reader.

RESULTS

We recently showed that introducing a single 2′-OMe (OMe) nucleotide at position 2 on the 5′-side of the gap can improve ASO therapeutic index by reducing toxicity (7). Given the importance of PS linkages for protein binding (14–16), we investigated if replacing one or more PS linkages with a neutral alkyl phosphonate linkage could also mitigate ASO toxicity without impacting potency. We replaced two PS in the 5′- and 3′-cEt wings and at the 5′- and 3′-side of the gap, of a toxic 3-10-3 cEt gapmer ASO A-SRB targeting mouse SRB1 mRNA, with MP and MOP linkages. In addition, we also prepared ASOs A-MP5 and A-MOP5 which had two MP or MOP linkages in the 3′- and the 5′-wings.

Synthesis of MP and MOP modified ASOs

The MP-linkages on DNA were introduced into the ASOs using commercially available amidites and standard synthesis conditions. The MOP-nucleoside building blocks were prepared as shown in Figure 1B. 3-Methoxypropylbromide was reacted with magnesium turnings to generate the corresponding Grignard reagent. Further reaction with the 1-chloro-*N*,*N*,*N*',*N*'-tetraisopropylphosphanediamine provided the phosphonamidite reagent which was isolated by extraction into hexanes and reacted with 5′-O-DMTr protected 2′-deoxy or cEt nucleosides to provide the desired phosphonamidites. The phosphonamidites were incorporated into oligonucleotides using standard coupling chemistry but deprotection using aqueous ammonia caused significant strand cleavage resulting in low yields of the final oligonucleotides. To avoid this, the ASOs with two incorporations of the MP or MOP-linkages were deprotected using modified conditions as described in the methods. Despite the use of the modified deprotection conditions, the final yields were lower for MP versus MOP modified ASOs. Presumably, the smaller size of the methyl group in MP allows for more efficient attack of the phosphorus atom by nucleophiles resulting in strand cleavage.

Biophysical and biological evaluation of MP and MOP ASOs targeting SRB1 mRNA

The MP and MOP modified ASOs were evaluated for their ability to stabilize oligonucleotide duplexes with complementary RNA (Figure 1C). All ASOs showed only slightly reduced duplex thermal stability relative to the parent ASO A-SRB with the exception of ASO A-MP1 with two MP linkages in the 5′-cEt wing. This ASO inexplicably showed significantly reduced duplex stability which was not observed with the corresponding MOP ASO A-MOP1. Overall, these data demonstrate that the MP or MOP linkage can be used in conjunction with cEt and DNA monomers without significant reductions in duplex thermal stability.

The MP and MOP ASOs were next evaluated in primary hepatocytes using free-uptake for ASO delivery to determine the concentration required to reduce SRB1 mRNA by 50% (IC_{50}, Figure 1C and F). Most ASOs showed excellent activity for reducing SRB1 mRNA suggesting that replacing two PS linkages with alkylphosphonate does not reduce the intrinsic activity of the ASO. ASOs MP1 and MOP1 showed slightly reduced activity as modification with alkyl phosphonates in the 5′-cEt wing affected RNA-affinity more adversely for these ASOs. ASOs A-MP5 and A-MOP5 that have four alkyl phosphonate linkages, also showed reduced activity relative to the parent A-SRB1 which could be a result of their reduced PS content. The PS-backbone enhances avidity for cell-surface proteins which can facilitate ASO entry and trafficking in cells (1,21).

The reduction of SRB1 mRNA expression in the liver of mice treated with these ASOs was evaluated. Balb-c mice were injected with increasing doses of the ASO and sacrificed 72 h after injection (Figure 1C and E). Livers were harvested and reduction in SRB1 mRNA was quantified with qRT-PCR. The levels of alanine amino transferases (ALT) in the plasma were also recorded as an indicator for hepatoxicity (Figure 1C and D). ASOs with 2 MP or MOP linkages in the 5′-wing or at the 3′-gap junction showed 2–3-fold reduced potency. In contrast, ASOs with MP or MOP at the 5′-gap junction or the 3′-wing showed comparable potency as the parent ASO. However, ASOs with four MP or MOP (A-MP5 and A-MOP) showed 4–5-fold reduced potency relative to the parent ASO. To determine if the above was a result of reduced ASO accumulation in the liver, we quantified levels of MOP-ASOs in the liver by HELISA (Figure 1G). ASO A-MOP5 showed the lowest accumulation relative to the other ASOs suggesting that reducing PS content below a threshold impacts ASO delivery and uptake, presumably by reducing interactions with cell-surface proteins which are responsible for the uptake of PS-ASOs in the liver (22). Most MP and MOP ASOs showed an improvement in therapeutic index relative to the parent ASO A-SRB (Figure 1C).

Since the MP and MOP ASOs above were evaluated in two independent experiments, we carried out a follow up study to evaluate the best MP and MOP ASOs in ahead to head experiment. Mice were injected with increasing doses of ASOs A-SRB, A-MP1 and A-MOP1 and knockdown of SRB1 mRNA in the liver and plasma ALT levels were measured post sacrifice (Figure 1H). All ASOs showed similar potency for reducing SRB1 mRNA but only the parent ASO showed ALT elevations at doses above 10 mg/kg. To determine if the MP and MOP ASOs showed similar accumulation in the liver, ASO concentration in the liver was quantified by LCMS where we observed minimal changes in accumulation for all three ASOs (Figure 1I). Thus, MP and MOP ASOs showed similar biological properties, but MOP ASOs exhibited improved chemical stability during synthesis and deprotection. As a result, subsequent work was only done using MOP ASOs.

Biological evaluation of ASOs with two MOP linkages targeting mouse CXCl12 mRNA

To determine if the results using the ASO A-SRB could be replicated using additional toxic ASOs targeting other genes in the liver, we systematically replaced two PS-linkages with MOP across the length of a toxic cEt gapmer ASO targeting CXCl12 mRNA (Figure 2). ASO A-CXC exhibits profound hepatoxicity in mice as evidence by elevated ALT levels in plasma after a single injection of 15 mg/kg and lethality at doses above 50 mg/kg. We also determined if ASOs which exhibit hepatotoxicity in mice would bind cellular proteins more tightly and cause nucleolar mislocalization of paraspeckle proteins such as P54nrb, leading to elevation of P21 mRNA, caspase activation and apoptosis in cells.

ASOs with two MOP linkages showed similar duplex stabilizing properties versus complementary RNA as the parent ASO A-CXC (Figure 2A). The MOP ASOs also showed similar potency for reducing CXCl12 mRNA in mouse 3T3L1 cells following delivery by electroporation (Figure 2A and Supplementary Figure S2). Elevation of P21 mRNA and caspase activation in cells were observed for all but four ASOs, AG12, AG23, AG34 and AG45, which had MOP incorporation near the 5′-end of the DNA-gap (Figure 2A–C). These ASOs also showed reduced global protein binding in a competition binding assay (Figure 2D). As

A

ASO	Sequence (5′-3′)	ΔTm °C/mod.	CXCl12 IC_{50} (nM)	P21 mRNA (% saline)	% nucleolar p54nrb	Caspase (% mock)	ALT (IU/L) 150 mg/kg	TD_{50} (mg/kg)	ED_{50} (mg/kg)	TI TD_{50}/ED_{50}
A-CXC	GCATGTTCTCACATTA	64.9	242	242	83	1378	FD	19	2.7	7
A-5W12	GxCxATGTTCTCACATTA	-1.1	110	357	ND	375	5139	179	7.3	25
A-5W23	GCxAxTGTTCTCACATTA	-1.3	117	306	ND	217	3117	289	4.1	70
A-5W3G1	GCAxTxGTTCTCACATTA	-2.3	155	238	ND	222	3041	211	7.7	27
A-G12	GCATxGxTTCTCACATTA	-2.4	214	109	11	72	30	safe	11.2	safe
A-G23	GCATGxTxTCTCACATTA	-2	263	121	25	113	27	safe	10.8	safe
A-G34	GCATGTxTxCTCACATTA	-1.8	133	105	23	64	29	safe	11	safe
A-G45	GCATGTTxCxTCACATTA	-2.5	188	137	26	167	29	safe	11.2	safe
A-G56	GCATGTTCxTxCACATTA	-2.2	137	214	78	295	5503	176	5.4	33
A-G67	GCATGTTCTxCxACATTA	-2.6	150	182	68	442	1380	308	8.2	38
A-G78	GCATGTTCTCxAxCATTA	-1.9	207	162	75	225	3423	197	8.6	23
A-G89	GCATGTTCTCAxCxATTA	-1.8	134	254	69	643	11954	84	4.3	20
A-G910	GCATGTTCTCACxAxTTA	-1.5	132	231	95	1074	FD	62	5.5	11
A-G10W1	GCATGTTCTCACAxTxTA	-1.2	162	272	ND	680	FD	52	3.2	16
A-3W12	GCATGTTCTCACATxTxA	-1	130	347	ND	945	FD	52	5.5	10

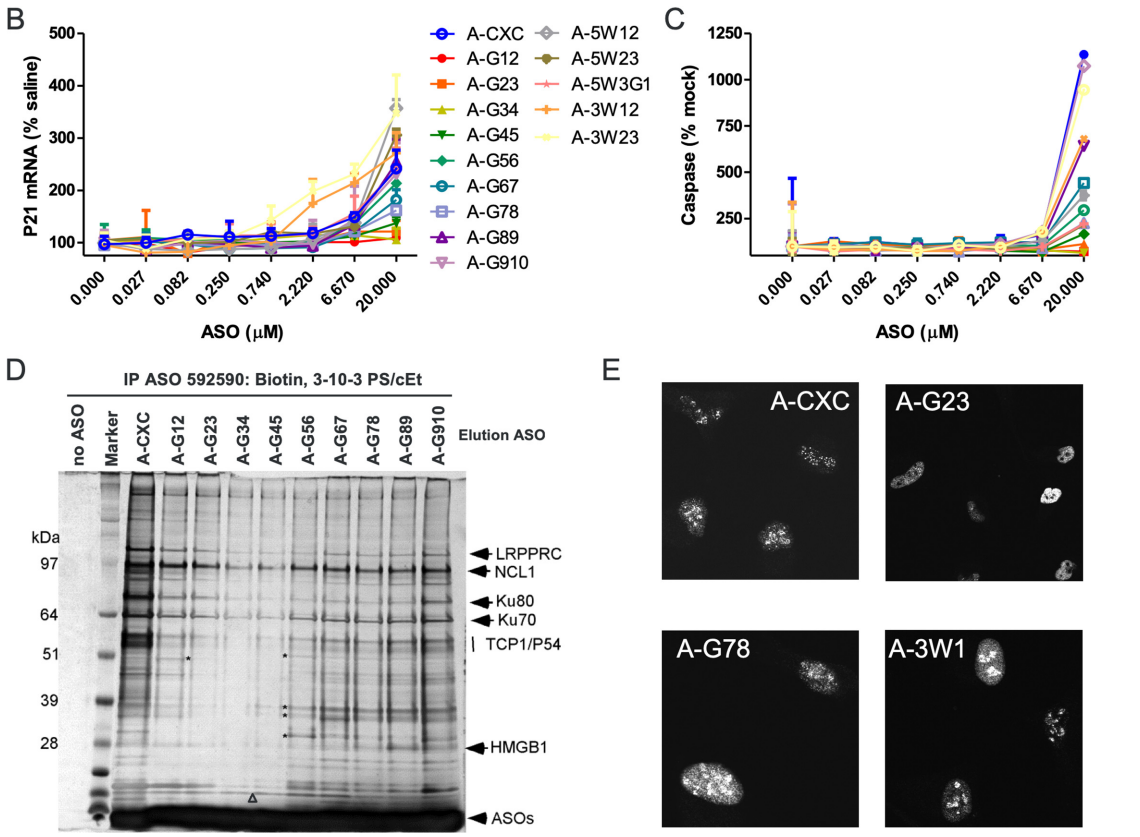

Figure 2. Site-specific introduction of two MOP-linkages near the 5′-end of the DNA gap reduces toxicity of a toxic gapmer ASO in cells and in mice. (**A**) Sequence, ASO design and chemistry (blue letters – cEt, black – PS DNA, red – MOP linkage); T_m for complementary RNA; Inhibition concentration (IC_{50}) for reducing CXCl12 mRNA by 50% in 3T3L1 cells; P21 mRNA elevation in 3T3L1 cells; and caspase activation in Hepa1-6 cells following ASO (20 μM) delivery by electroporation; plasma ALT (IU/L) in mice 72 hours after injection of 150 mg/kg ASO; ASO dose (mg/kg) required to produce half-maximal elevations in plasma ALT (TD_{50}); and effective dose (mg/kg) for reducing CXCl12 mRNA in mouse liver by 50% (ED_{50}). Columns were formatted using the conditional formatting option in MS excel using the red-white-blue color scale. Blue indicates reduced toxicity and improved activity while red indicates enhanced toxicity and reduced activity respectively. Therapeutic index (TI) was calculated as the ratio of TD_{50} divided by the ED_{50}. ASOs were deemed safe if no elevation in plasma ALT were observed at the highest dose tested. (**B**) qRT-PCR quantification of P21 mRNA levels in 3T3L1 cells treated with ASOs at indicated concentrations by electroporation. Errors are ±std.dev. (**C**) Caspase activity levels in Hepa1-6 cells treated by electroporation with different ASOs at indicated concentrations for 18–24 h. Errors are ±std.dev. (**D**) PS-ASO-binding proteins were isolated from HeLa lysate with 5′-biotinylated PS-ASOs and were eluted by competition using unconjugated MOP-ASOs. Silver staining of eluted proteins resolved on SDS-PAGE. L, size marker. (**E**) Toxic ASOs A-CXC, A-3W1 and A-G78 causes mislocalization of P54nrb to the nucleolus after transfection into HeLa cells (200 nM for 2 h) while the safe MOP ASO A-G23 does not. FD = found dead.

predicted by the toxicity model, all the ASOs which caused 2-fold or greater caspase elevation relative to mock treated cells showed mislocalization of paraspeckle protein P54nrb to the nucleolus in cells (Figure 2E and Supplementary Figure S3).

To determine if the observations in cells translate to animals, mice were injected with 150 mg/kg of the CXCl12 ASOs (Figure 2A). Only ASOs AG12, AG23, AG34 and AG45 that were predicted to be safe in the cellular assays were found to be safe in mice. The rest of the ASOs showed significant ALT elevations and even lethality in mice. The ASOs were also evaluated for potency to reduce CXCl12 mRNA in the liver. Mice were injected with increasing doses of MOP ASOs and sacrificed 72 h after injection. Livers were harvested, and the dose required to reduce CXCl12 mRNA by 50% in the liver was determined. Most MOP ASOs showed 2-fold reduced potency relative to the control ASO A-CXC but the safest ASOs AG12, AG23, AG34 and AG45 showed almost 4-fold reduced potency (Figure 2A and Supplementary Figure S2). To confirm that the reduced activity in mice with some MOP ASOs was not because of reduced cellular uptake, the gap-modified MOP ASOs were evaluated by free-uptake in primary hepatocytes where they exhibited similar potencies as the parent ASO A-CXC (Supplementary Figure S4). These results suggested that replacing two PS-linkages near the 5′-side of the DNA-gap with MOP can enhance ASO safety, but may reduce potency for some ASO sequences in mice.

Biological evaluation of ASOs with one MOP linkages targeting mouse CXCl12 mRNA

To determine if using fewer MOP-linkages could enhance ASO safety without incurring a significant penalty for activity, we sequentially replaced a single PS-linkage in ASO A-CXC with MOP (Figure 3). All the RNA/ASO duplexes with single MOP incorporation exhibited comparable melting temperature (T_m) suggesting similar binding affinities of MOP-ASOs for the target mRNA (Figure 3A). To confirm that all the MOP ASOs support cleavage by RNaseH1, ASO/RNA duplexes were evaluated in a cleavage assay where the MOP ASOs showed similar cleavage rates relative to parent ASO A-CXC (Figure 3B). ASOs with single MOP also exhibited similar activity for reducing CXCl12 mRNA in 3T3L1 cells as the parent ASO A-CXC (Figure 3A and Supplementary Figure S5). Introducing MOP at gap-positions 2 and 3 mitigated P21 mRNA elevation and caspase activation (Figure 3A and Supplementary Figure S6) and nucleolar mislocalization of P54nrb (Supplementary Figure S7) in cells indicative of reduced cytotoxicity. In mice, a single MOP linkage at position 2 or 3 (A-G2 and A-G3) in the DNA gap eliminated hepatotoxicity, while the rest of the MOP ASOs still exhibited profound toxicity and even lethality with a single injection of 150 mg/kg ASO (Figure 3A).

Consistent with the protein interaction hypothesis, safe MOP ASO A-G2 associated with significantly less proteins than the parent ASO A-CXC (Figure 3C). To determine if MOP ASOs which cause toxicity in mice co-localize with P54nrb in the nucleolus, we transfected Cy3-labeled parent ASO A and MOP ASOs (A-G1, A-G2, A-G3, A-G4 and A-G9) into HeLa cells. Cy3-ASOs with MOP at gap-positions 2 and 3 did not cause nucleolar mislocalization of P54nrb (Figure 3D and Supplementary Figures S8 and S9), while Cy3-ASOs with MOP at gap-positions 1, 4 and 9 caused nucleolar mislocalization of P54nrb. ASOs with MOP at gap-positions 1, 4 and 9 (but not 2 and 3) also showed significant cytotoxicity in HeLa cells, as seen from the number of surviving cells after treatment with the different ASOs (Supplementary Figure S10).

The effect of introducing a single MOP in the DNA-gap on antisense activity in mice was also examined. Mice were injected subcutaneously with increasing doses of ASOs and the dose required to reduce CXCl12 mRNA by 50% in the liver was calculated (Figure 3A and Supplementary Figure S5). Several MOP ASOs exhibited ∼2-fold reduction in potency relative to the parent ASO A. ASOs with a single MOP in the cEt wings were not evaluated in the dose-response study above as all of them showed significant hepatotoxicity in the single dose ALT screening study (Figure 3A). To confirm that the reduced potency in mice was not a result of impaired uptake into hepatocytes, the MOP ASOs were evaluated in primary mouse hepatocytes by free uptake where they exhibited similar potency as the parent ASO A-CXC (Supplementary Figure S4).

To determine if potency of the safe MOP ASOs could be improved by targeted delivery to hepatocytes in mice, we evaluated the GalNAc conjugates (23) of the parent ASO (A-GN3) and the MOP ASOs (A2-GN3 and A23-GN3) in mice (Figure 3E). All ASOs showed >10-fold enhancement in potency, but only ASOs with MOP at gap-position 2 mitigated toxicity and provided a dramatic improvement in safety thus extending the predictive value of the toxicity model to include MOP at position 2 and GalNAc-ASO conjugates.

A single MOP linkage at position 2 in the DNA gap reduces toxicity for multiple ASOs

To determine if introducing a MOP at position 2 could reduce toxicity of other ASO sequences, we evaluated five toxic ASOs versus four additional gene targets in mice (Figure 4). The ASOs were evaluated as GalNAc conjugates (Figure 4B), which enhance ASO potency 10-fold in the liver by targeted delivery via the ASGR. The toxic parent and MOP-modified GalNAc-ASOs were injected into mice at 50 mg/kg, which would correspond to a dose of 500 mg/kg for the unconjugated ASOs. All the parent cEt gapmer ASOs showed elevations in plasma ALT levels while the MOP-modified ASOs were not toxic (Figure 4A). Three ASOs were further evaluated by dose-response to determine the effect of MOP on potency and therapeutic index (Figure 4C–E). The MOP ASOs exhibited slight reduction in potency but enhancement in therapeutic index relative to their parent controls. These experiments further validated that the effect of MOP-modification is sequence independent and applicable broadly across multiple ASO sequences and gene targets.

A

ASO	Sequence (5'-3')	ΔTm °C/mod.	CXCl12 IC_{50} (nM)	P21 mRNA (% saline)	% nucleolar p54nrb	Caspase (% mock)	ALT (IU/L) 150 mg/kg	TD_{50} (mg/kg)	ED_{50} (mg/kg)	TI TD_{50}/ED_{50}
A-CXC	GCATGTTCTCACATTA	64.9	242	242	83	1378	FD	19	2.9	7
A-5W1	GxCATGTTCTCACATTA	-1.3	189	210	82	753	3788	NT	NT	NT
A-5W2	GCxATGTTCTCACATTA	0.1	138	184	86	580	4149	NT	NT	NT
A-5W3	GCAxTGTTCTCACATTA	-0.7	65	203	90	643	FD	NT	NT	NT
A-G1	GCATxGTTCTCACATTA	-1.2	145	152	38	240	7764	148	4.5	33
A-G2	GCATGxTTCTCACATTA	-1	275	128	30	113	46	safe	6.8	safe
A-G3	GCATGTxTCTCACATTA	-1.4	396	100	31	94	44	safe	6.2	safe
A-G4	GCATGTTxCTCACATTA	-1.9	315	142	42	243	4481	190	5.7	33
A-G5	GCATGTTCxTCACATTA	-2	115	159	85	629	9139	124	5.1	24
A-G6	GCATGTTCTxCACATTA	-1.1	143	262	88	1253	17846	52	3.6	14
A-G7	GCATGTTCTCxACATTA	-1.6	203	250	76	569	12510	76	4.4	17
A-G8	GCATGTTCTCAxCATTA	-0.8	107	185	78	868	FD	61	4.3	14
A-G9	GCATGTTCTCACxATTA	-1	121	218	85	983	FD	61	3.1	20
A-G10	GCATGTTCTCACAxTTA	-1.1	133	235	94	1405	FD	42	2.1	20
A-3W1	GCATGTTCTCACATxTA	0.8	110	257	82	1282	FD	NT	NT	NT
A-3W2	GCATGTTCTCACATTxA	-0.5	155	219	89	1596	FD	NT	NT	NT

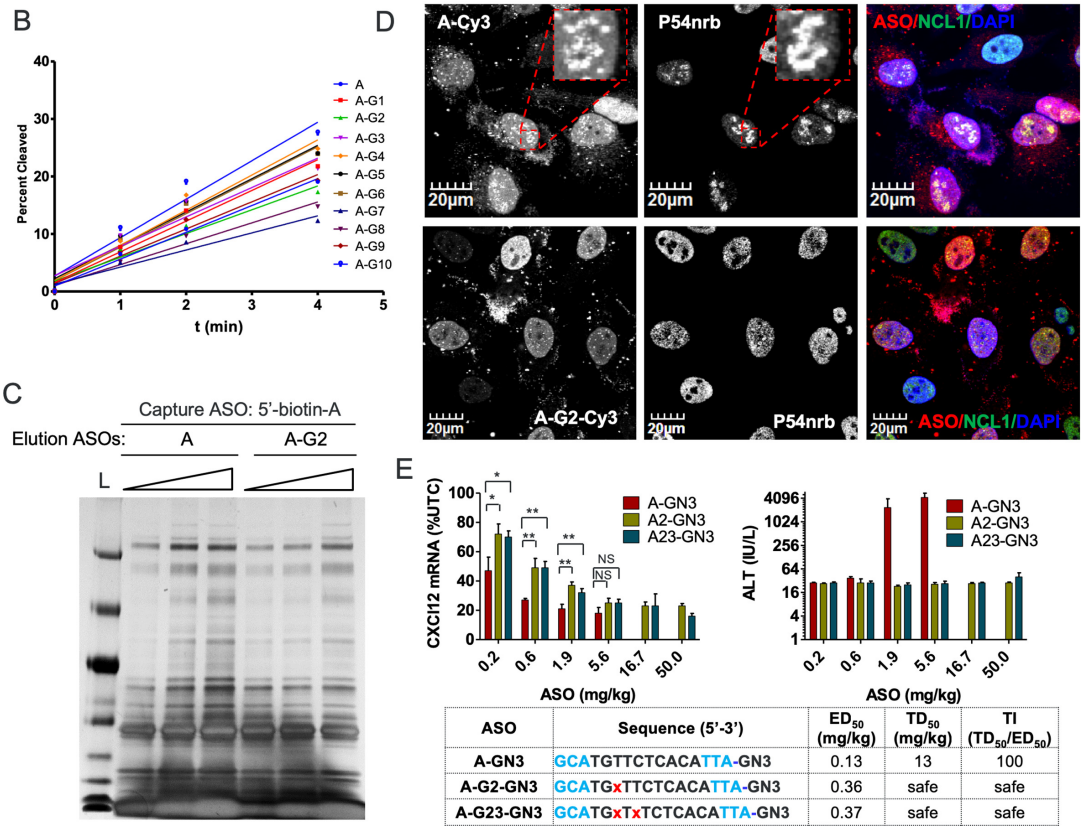

ASO	Sequence (5'-3')	ED_{50} (mg/kg)	TD_{50} (mg/kg)	TI (TD_{50}/ED_{50})
A-GN3	GCATGTTCTCACATTA-GN3	0.13	13	100
A-G2-GN3	GCATGxTTCTCACATTA-GN3	0.36	safe	safe
A-G23-GN3	GCATGxTxTCTCACATTA-GN3	0.37	safe	safe

Figure 3. Replacing PS with a single MOP-linkage at gap positions 2 and 3 reduces toxicity without impacting the potency of a toxic gapmer ASO in cells and in mice. (**A**) Sequence, ASO design and chemistry (blue letters – cEt, black – PS DNA, red – MOP linkage); T_m for complementary RNA; Inhibition concentration (IC_{50}) for reducing CXCl12 mRNA by 50% in 3T3L1 cells; P21 mRNA elevation in 3T3L1 cells; and caspase activation in Hepa1-6 cells following ASO (20 μM) delivery by electroporation; plasma ALT (IU/l) in mice 72 h after injection of 150 mg/kg ASO; ASO dose (mg/kg) required to produce half-maximal elevations in plasma ALT (TD_{50}); and ED_{50} (mg/kg) for reducing CXCl12 mRNA in mouse liver. Columns were formatted using the conditional formatting option in MS excel using the red-white-blue color scale. Blue indicates reduced toxicity and improved activity while red indicates enhanced toxicity and reduced activity respectively. Therapeutic index (TI) was calculated as the ratio of TD_{50} divided by the ED_{50}. ASOs were deemed safe if no elevation in plasma ALT were observed at the highest dose tested. (**B**) Initial rates for cleavage of MOP-ASO/RNA duplexes by human recombinant RNaseH1. (**C**) PS-ASO-binding proteins were isolated from HeLa lysate with 5′-biotinylated PS-ASOs and were eluted by competition using unconjugated PS-ASOs at three different elution concentrations. Silver staining of eluted proteins resolved on SDS-PAGE. L, size marker. (**D**) ASO A-Cy3 causes mislocalization of P54nrb to the nucleolus after transfection into Hela cells (200 nM for 2 hours) while the MOP ASO A2-Cy3 does not. (**E**) ED_{50} for reducing CXCl12 mRNA in the liver in mice using GalNAc conjugates of select MOP ASOs. Balb-c mice were injected subcutaneously with a single dose of 0.2, 0.6, 1.8 and 5.4 mg/kg of A-GN3 or with 0.2, 0.6, 1.8, 5.4, 15 and 50 mg/kg of A2-GN3 or A23-GN3. Mice were sacrificed after 72 h and plasma ALT levels were recorded. Livers were homogenized and reduction of CXCl12 mRNA was measured by qRT-PCR. Errors are ±std.dev. P-values were calculated based on unpaired *t*-test using Prism. $^*P < 0.05$; $^{**}P < 0.01$; NS, not significant. FD = found dead. NT = not tested.

A

Target	ASO	Sequence (5'-3')	ALT (IU/L) 50 mg/kg
FBO1a	GN3-ASO	GGACTGAAATAGCAGA-GN3	1467 (416)
	GN3-MOP	GGACTxGAAATAGCAGA-GN3	102 (64)
HDAC2	GN3-ASO	ACCCTCAAGTCTCCTG-GN3	3655 (1052)
	GN3-MOP	ACCCTxCAAGTCTCCTG-GN3	6 (6)
HDAC2	GN3-ASO	TAGTCTCTGTCAGTTA-GN3	2370 (1582)
	GN3-MOP	TAGTCxTCTGTCAGTTA-GN3	30 (1)
FXI	GN3-ASO	GTCAGTATCCCAGTGT-GN3	1555 (545)
	GN3-MOP	GTCAGxTATCCCAGTGT-GN3	43 (17)
Dynamin2	GN3-ASO	AGACTCTCGGTTCCGA-GN3	1058 (288)
	GN3-MOP	AGACTxCTCGGTTCCGA-GN3	25 (4)

B

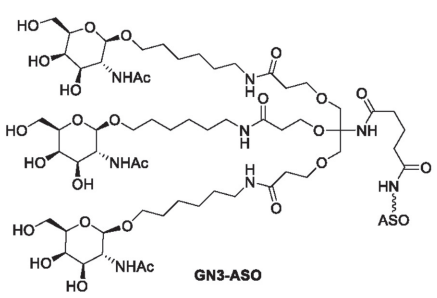

C

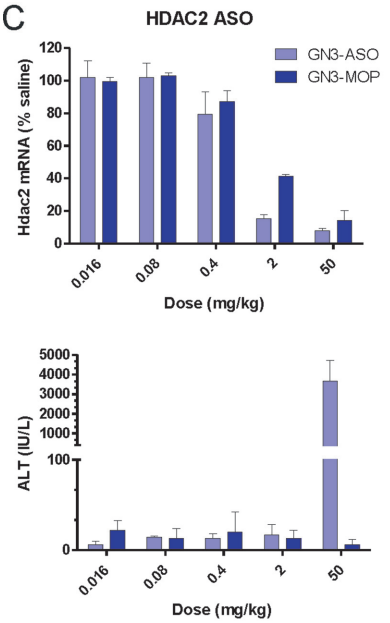

D

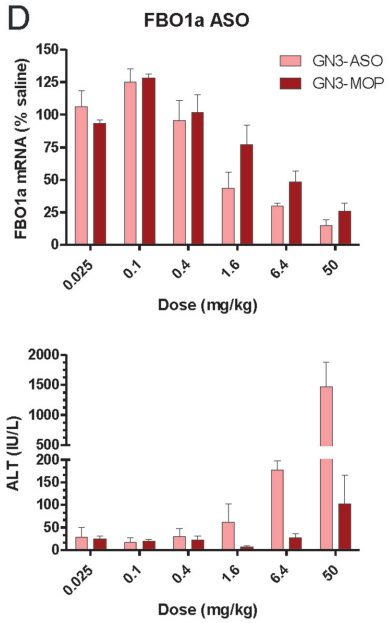

E

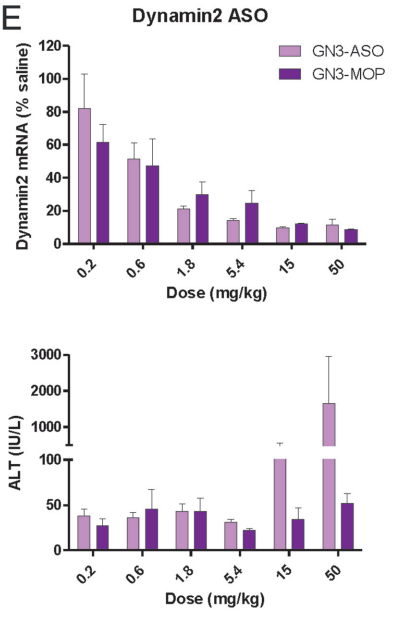

Target	ASO	ED_{50}	TD_{50}	TI
HDAC2	GN3-ASO	0.8	65	81
	GN3-MOP	1.3	safe	safe

Target	ASO	ED_{50}	TD_{50}	TI
FBO1a	GN3-ASO	1.2	371	309
	GN3-MOP	3.3	1758	532

Target	ASO	ED_{50}	TD_{50}	TI
Dyn2	GN3-ASO	0.7	213	304
	GN3-MOP	0.5	safe	safe

Figure 4. MOP at gap position 2 reduces toxicity of ASOs targeting diverse gene targets. (**A**) Balb-c mice were injected subcutaneously with the parent GalNAc (GN3) gapmer ASOs or their MOP-counterparts at 50 mg/kg. Mice were sacrificed after 72 h and plasma ALT (IU/l) levels were measured. (**B**) Structure of GN3-conjugated ASOs. Therapeutic indices of parent and MOP GN3-ASOs targeting (**C**) mouse HDAC2 mRNA, (**D**) FBO1a mRNA (**E**) Dynamin2 mRNA. Balb-c mice were injected subcutaneously with increasing doses of the ASOs as indicated. Mice were sacrificed 72 h after injection and plasma ALT levels were measured to determine the TD_{50}. Livers were homogenized, and reduction of the targeted mRNA were quantified by qRT-PCR and ED_{50} (mg/kg) was determined. All errors are ±std.dev.

Structural analysis to rationalize changes in RNaseH1 cleavage patterns for MOP ASO/RNA duplexes

We next carried out a structural analysis to better understand how site-specific incorporation of a neutral linkage could modulate interactions with proteins by using RNaseH1 as a model protein. Introducing MOP in the DNA-gap produced dramatic changes in cleavage patterns on the ASO/RNA duplex (Figure 5A and Supplementary Figure S11). Human RNaseH1 cleaved the RNA strand in the parent ASO A-CXC/RNA duplex at six distinct sites which were labeled a–f respectively. Insertion of MOP across the DNA-gap led to significant changes in cleavage patterns. The changes in cleavage patterns could be rationalized by considering the distinct but overlapping seven nucleotide footprint of the catalytic domain of RNaseH1 on the ASO/RNA duplex for each cleavage site on the RNA (Figure 5B, region shaded gray) (24). For example, insertion of MOP at C7 in the gap ablates cleavage at sites a, b, c but enhances cleavage at sites d, e and f relative to the parent ASO A-CXC. Overlaying this information on the footprint for each cleavage site suggests that inserting a neutral linkage like MOP at positions 3, 4 or 5 of the footprints ablates cleavage by RNaseH1 (Figure 5C).

The crystal structure of the catalytic domain of human RNaseH1 bound to a DNA/RNA duplex (Figure 5D) shows that the enzyme makes contact with the third, fourth and fifth phosphate linkages in the DNA strand for each cleavage site on the RNA (25). The enzyme contacts the third phosphate in the phosphate binding pocket via electrostatic interactions with Arg179, the fourth phosphate via

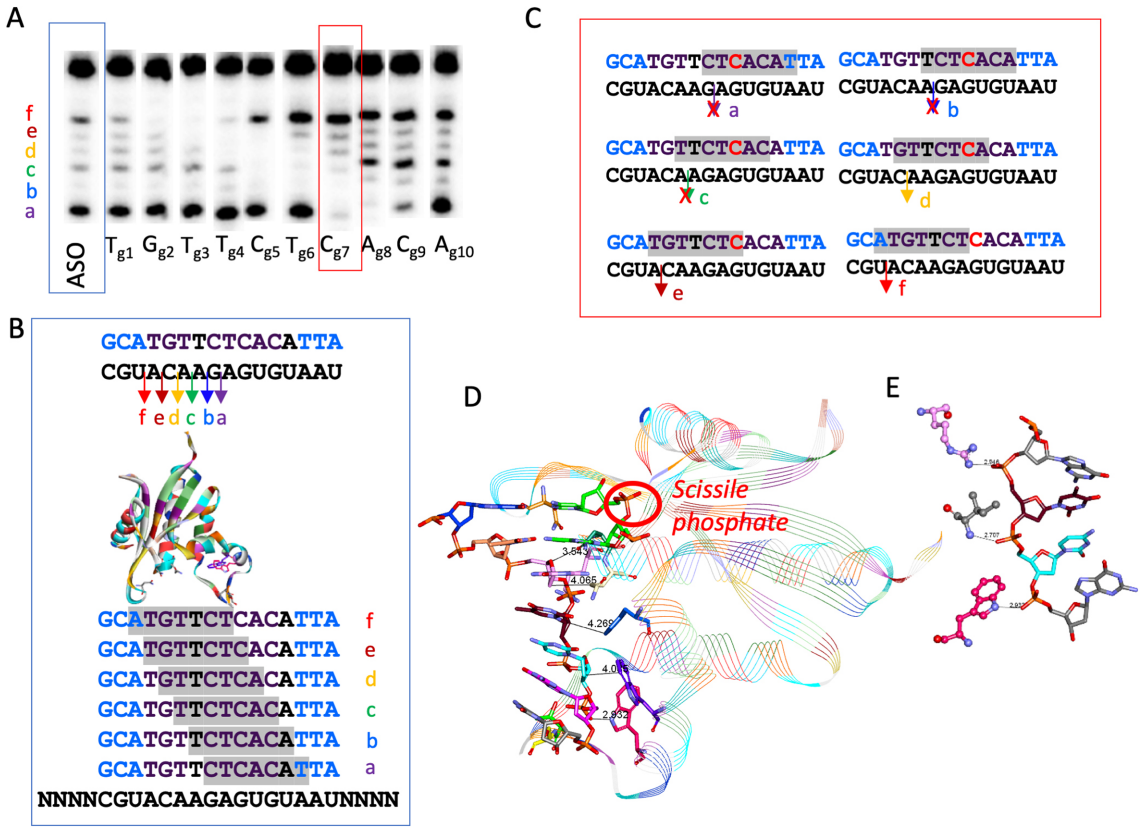

Figure 5. Structural rationale for the changes in RNaseH1 cleavage patterns for MOP-ASO/RNA duplexes (**A**) Human RNaseH1 cleaves the parent ASO A-CXC/RNA duplex at six distinct sites (a–f) and site-specific incorporation of MOP produced distinct changes in RNaseH1 cleavage patterns. (**B**) The distinct but overlapping 7-nucleotide footprints of the catalytic domain of human RNaseH1 for cleavage sites a–f. (**C**) Insertion of MOP at C7 in the gap ablates cleavage sites a, b and c indicating that MOP is not tolerated at positions 3, 4 and 5 of the seven-nucleotide footprint. (**D**) Structure of the catalytic domain of human RNaseH1 with the scissile site on the RNA (only two nucleotides flanking the scissile site are shown for clarity). The catalytic domain makes three critical contacts with the backbone phosphates at positions 3, 4 and 5 of the footprint. (**E**) Insertion of neutral linkages at positions 3, 4 and 5 of the footprint ablates RNaseH1 cleavage.

an H-bond with the backbone amide of Ile239 and the fifth phosphate through an H-bonding interaction with the aromatic NH of Trp225. Replacing the anionic phosphate (or phosphorothioate) linkage with a neutral linkage like MOP at positions 3, 4 and 5 interferes with these important contacts and ablates cleavage (Figure 5E). In contrast, placing the neutral linkage at positions 1, 2, 6 and 7 are tolerated and does not ablate cleavage. This analysis showed that even small structural perturbations can produce dramatic changes in ASO-protein interactions using an important ASO-binding protein. Conceivably, chemical changes in the ASO can have similar effects to modulate interactions of PS ASOs with other intra-cellular proteins.

DISCUSSION

Chemical modification of ASOs can improve their pharmacological profile by enhancing nuclease stability, mechanistic potency and pharmacokinetic properties (26). PS-ASOs represent an important class of pharmaceutical agents with 4 approved drugs and over 40 ASOs at various stages of clinical development (27). The vast majority of PS-gapmer ASOs in the clinic are also modified using the 2′-*O*-methoxyethyl RNA (MOE) modification (28). We and others have shown that replacing MOE with conformationally restricted and hydrophobic modifications such as LNA and cEt can enhance ASO potency in animal models (29,30). However, a subset of LNA and cEt ASOs have shown an increased risk for causing hepatotoxicity (31). While it is possible to identify safe and efficacious cEt gapmer ASOs, several of which have advanced into the clinic (32), screening out toxic ASO leads represents a considerable resource burden during preclinical development. Thus, identifying the mechanism/s by which these ASOs cause toxicities and general chemical strategies to mitigate these toxicities could greatly simplify their development as potential therapeutic agents.

The mechanism by which some MOE, LNA/cEt PS gapmer ASOs show toxicity has been a subject of debate in the literature and recent research has implicated certain sequence motifs (33,34), non-specific reduction of genes with long introns (35) or with very long pre-mRNA transcripts (36), disruption of endosomal pathways (37), and nonspecific protein binding (38) as potential mechanisms for toxicity. We showed that toxic PS ASOs show enhanced binding to cellular proteins as compared to safe ASOs, resulting in RNaseH1-dependent nucleolar mislocalization of paraspeckle proteins, nucleolar stress and fragmentation, upregulation of P21 mRNA, and activation of caspase ac-

tivity indicative of apoptosis (7). Site-specific introduction of OMe at position 2 in the gap reduced binding to cellular proteins and mitigated toxicity without affecting activity. As an extension of that work, we now show that replacing a PS linkage with a neutral linkage at position 2 or 3 in the DNA-gap can also mitigate toxicity by modulating interactions with cellular proteins.

Replacing one or two PS linkages with a neural alkyl phosphonate had a minimal effect on the thermal stability of the ASO/RNA duplexes suggesting that the phosphonate modifications do not adversely affect RNA-binding properties. ASOs with one or two MOP modification showed very similar potency in primary hepatocytes when delivered by free-uptake suggesting that the modification does not impede the ability of the ASO to interact with cell-surface proteins which are responsible for ASO uptake into hepatocytes. However, ASOs with four MOP linkages showed reduced tissue accumulation suggesting that reducing the number of PS linkages below a certain threshold can affect tissue accumulation, presumably be modulating interactions with plasma proteins which facilitate distribution of the ASO from the injection site to peripheral tissues (14).

Once internalized into cells, PS ASOs interact with a host of cellular proteins including proteins in various nuclear compartments (1). However, toxic ASOs bind more proteins including paraspeckle proteins such as P54nrb causing them to be mislocalized to the nucleolus. This can lead to nucleolar stress and fragmentation and eventually apoptosis as evidenced by upregulation of P21 mRNA and caspase activation. This hypothesis was corroborated by microscopy data which showed that the toxic MOP ASOs colocalize with P54nrb in the nucleolus while the safe MOP ASOs do not. The positional preference for MOP placement at the 5′-end of the gap is consistent with our previous findings that many proteins, including P54nrb, FUS and other paraspeckle and nucleolar proteins, interact with the 5′′ cEt wing/DNA gap region of PS ASOs (4).

Unlike interactions of small molecules with proteins which typically occurs in hydrophobic binding pockets or crevices, the interaction of single or double stranded nucleic acids with proteins often occurs along an extended interface with multiple points of contact between the nucleic acid and the protein (25,39). Indeed, cellular proteins interact with nucleic acids via electrostatic, hydrophobic and H-bonding interactions in a sequence-dependent or -independent manner (40,41). Conceivably, toxic PS ASOs can template interactions between proteins such as P54nrb and RNaseH1 leading to phase separation and nucleolar mislocalization resulting in cytotoxicity. The ability of a single neutral linkage to disrupt these interactions is remarkable but not improbable. For example, even though the catalytic and HBD of RNaseH1 make several H-bonding, electrostatic and hydrophobic interactions with the nucleic acid, introduction of a single neutral linkage can produce dramatic changes in RNaseH1 cleavage patterns by modulating one or more of these interactions.

An alternate explanation for reducing cytotoxicity is that introduction of the neutral linkage suppresses cleavage of off-target mRNA bound ASO duplexes by RNaseH1 leading to fewer off-target effects (24). However, safe and toxic ASOs have similar number of binding sites on putative off-target mRNA (42) and RNaseH1 typically produces multiple cleavage sites for every ASO/RNA duplex. Thus, it is less likely that all off-target mRNA are cleaved in the same manner such that they can be blocked by the same modification strategy. Furthermore, apoptosis can cause global reduction of cellular mRNA, resulting in a similar phenotype as that observed after treating cells or mice with toxic ASOs (43).

We recently showed that replacing PS DNA at gap-position 2 from the 5′-wing junction with 2′-modifications can also improve the TI of gapmer ASOs (7). We also showed that these results were general for ASOs with wing chemistries such as MOE, cEt and LNA. Thus, gap-modification strategies could be used to improve the safety of potential ASO drug candidates during pre-clinical development. Alternatively, these strategies may permit accessing mRNA sequence space, targeting which otherwise produces active but toxic ASO sequences. Site-specific incorporation of neutral alkyl phosphonate linkages can also be useful for modulating the therapeutic properties of nucleic acids which utilize alternate antisense mechanisms such as splice correction, siRNA, miRNA and CRISPR, as they can be combined with sugar modifications used to improve the drug-like properties of therapeutic nucleic acids (26).

The ability to use chemical modifications in a site-specific manner to produce profound changes in the biological behavior of therapeutic oligonucleotides is remarkable. This can allow medicinal chemists to use the entire palette of chemical modifications available in the oligonucleotide chemistry toolbox to engineer specific properties into therapeutic nucleic acids. For example, modifications which produce slight reductions in RNA affinity but otherwise modulate local structural perturbations like backbone deformations, sugar pucker and hydrophobicity, cannot be incorporated multiple times into oligonucleotides without incurring a significant reduction in RNA-affinity and antisense activity. However, most of these modifications might be tolerated as single insertions if they can modulate the biological behavior of an oligonucleotide drug in a desirable manner. Similarly, the cellular cytotoxicity assays and endpoints described in this work can be used to triage a large number of potential drug candidates for cytotoxicity before intiating rodent tolerability studies.

In conclusion, we show that fine tuning the size, hydrophobicity and position of chemical modifications within the PS DNA-gap region can profoundly affect ASO behavior by modulating ASO/protein interactions causative of cellular toxicity. Further identification of the binding motifs and amino acids involved in the interactions of ASOs with key cellular proteins can help build robust models of these interactions. Furthermore, controlling these molecular recognition events can direct ASO localization to specific cellular compartments (6,44) and further enhance the therapeutic properties of PS ASOs.

SUPPLEMENTARY DATA

Supplementary Data are available at NAR Online.

FUNDING

Ionis Pharmaceuticals. Funding for open access charge: Ionis Pharmaceuticals.
Conflict of interest statement. None declared.

REFERENCES

1. Crooke,S.T., Wang,S., Vickers,T.A., Shen,W. and Liang,X-h. (2017) Cellular uptake and trafficking of antisense oligonucleotides. *Nat. Biotech.*, **35**, 230–237.
2. Seth,P.P., Tanowitz,M. and Bennett,C.F. (2019) Selective tissue targeting of synthetic nucleic acid drugs. *J.Clin.Investig.*, **129**, 915–925.
3. Liang,X-h., Sun,H., Shen,W. and Crooke,S.T. (2015) Identification and characterization of intracellular proteins that bind oligonucleotides with phosphorothioate linkages. *Nucleic Acids Res.*, **43**, 2927–2945.
4. Liang,X.-H., Shen,W., Sun,H., Kinberger,G.A., Prakash,T.P., Nichols,J.G. and Crooke,S.T. (2016) Hsp90 protein interacts with phosphorothioate oligonucleotides containing hydrophobic 2′-modifications and enhances antisense activity. *Nucleic Acids Res.*, **44**, 3892–3907.
5. Shen,W., Liang,X-h. and Crooke,S.T. (2014) Phosphorothioate oligonucleotides can displace NEAT1 RNA and form nuclear paraspeckle-like structures. *Nucleic Acids Res.*, **42**, 8648–8662.
6. Liang,X-h., Shen,W., Sun,H., Prakash,T.P. and Crooke,S.T. (2014) TCP1 complex proteins interact with phosphorothioate oligonucleotides and can co-localize in oligonucleotide-induced nuclear bodies in mammalian cells. *Nucleic Acids Res.*, **42**, 7819–7832.
7. Shen,W., DeHoyos,C.L., Migawa,M.T., Vickers,T.A., Sun,H., Low,A., Bell,T.A. III, Rahdar,M., Mukhopadhyay,S., Hart,C.E. *et al.* (2019) Chemical modification of PS-ASO therapeutics reduces cellular protein-binding and improves the therapeutic index. *Nat. Biotechnol.*, doi:10.1038/s41587-019-0106-2.
8. Altmann,K.-H., Dean,N.M., Fabbro,D., Freier,S.M., Geiger,T., Hanera,R., Hiisken,D.A., Martina,P., Monia,B.P.B., Miiller,M. *et al.* (1996) Second Generation of Antisense Oligonucleotides: From Nuclease Resistance to Biological Efficacy in Animals. *CHIMIA Int. J. Chem.*, **50**, 168–176.
9. Obika,S., Nanbu,D., Hari,Y., Andoh,J.-I., Morio,K.-I., Doi,T. and Imanishi,T. (1998) Stability and structural features of the duplexes containing nucleoside analogs with a fixed N-type conformation, 2′-O,4′-C-methyleneribonucleosides. *Tetrahedron Lett.*, **39**, 5401–5404.
10. Wengel,J. (1999) Synthesis of 3′-C- and 4′-C-branched oligodeoxynucleotides and the development of locked nucleic acid (LNA). *Acc. Chem. Res.*, **32**, 301–310.
11. Seth,P.P., Vasquez,G., Allerson,C.A., Berdeja,A., Gaus,H., Kinberger,G.A., Prakash,T.P., Migawa,M.T., Bhat,B. and Swayze,E.E. (2010) Synthesis and biophysical evaluation of 2′,4′-constrained 2′O-methoxyethyl and 2′,4′-constrained 2′O-ethyl nucleic acid analogues. *J. Org. Chem.*, **75**, 1569–1581.
12. Cerritelli,S.M. and Crouch,R.J. (2009) Ribonuclease H: the enzymes in eukaryotes. *FEBS J.*, **276**, 1494–1505.
13. Lima,W.F., Wu,H. and Crooke,S.T. (2001) Human RNases H. *Methods Enzymol.*, **341**, 430–440.
14. Gaus,H.J., Gupta,R., Chappell,A.E., Østergaard,M.E., Swayze,E.E. and Seth,P.P. (2018) Characterization of the interactions of chemically-modified therapeutic nucleic acids with plasma proteins using a fluorescence polarization assay. *Nucleic Acids Res.*, **47**, 1110–1122.
15. Vickers,T.A. and Crooke,S.T. (2016) Development of a Quantitative BRET Affinity Assay for Nucleic Acid-Protein Interactions. *PLoS ONE*, **11**, e0161930.
16. Gaus,H., Miller,C.M., Seth,P.P. and Harris,E.N. (2018) Structural Determinants for the Interactions of Chemically Modified Nucleic Acids with the Stabilin-2 Clearance Receptor. *Biochemistry*, **57**, 2061–2064.
17. Miller,P.S., Yano,J., Yano,E., Carroll,C., Jayaraman,K. and Ts'o,P.O.P. (1979) Nonionic nucleic acid analogs. Synthesis and characterization of dideoxyribonucleoside methylphosphonates. *Biochemistry*, **18**, 5134–5143.
18. Reynolds,M.A., Hogrefe,R.I., Jaeger,J.A., Schwartz,D.A., Riley,T.A., Marvin,W.B., Daily,W.J., Vaghefi,M.M., Beck,T.A., Knowles,S.K. *et al.* (1996) Synthesis and Thermodynamics of Oligonucleotides Containing Chirally Pure RP Methylphosphonate Linkages. *Nucleic Acids Res.*, **24**, 4584–4591.
19. Wu,H., Lima,W.F. and Crooke,S.T. (1999) Properties of cloned and expressed human RNase H1. *J. Biol. Chem.*, **274**, 28270–28278.
20. Yu,R.Z., Baker,B., Chappell,A., Geary,R.S., Cheung,E. and Levin,A.A. (2002) Development of an ultrasensitive noncompetitive hybridization-ligation enzyme-linked immunosorbent assay for the determination of phosphorothioate oligodeoxynucleotide in plasma. *Anal. Biochem.*, **304**, 19–25.
21. Miller,C.M., Donner,A.J., Blank,E.E., Egger,A.W., Kellar,B.M., Ostergaard,M.E., Seth,P.P. and Harris,E.N. (2016) Stabilin-1 and Stabilin-2 are specific receptors for the cellular internalization of phosphorothioate-modified antisense oligonucleotides (ASOs) in the liver. *Nucleic Acids Res.*, **44**, 2782–2794.
22. Miller,C.M., Tanowitz,M., Donner,A.J., Prakash,T.P., Swayze,E.E., Harris,E.N. and Seth,P.P. (2018) Receptor-mediated uptake of phosphorothioate antisense oligonucleotides in different cell types of the liver. *Nucleic Acid Ther.*, **28**, 119–127.
23. Prakash,T.P., Yu,J., Migawa,M.T., Kinberger,G.A., Wan,W.B., Ostergaard,M.E., Carty,R.L., Vasquez,G., Low,A., Chappell,A. *et al.* (2016) Comprehensive structure-activity relationship of triantennary N-acetylgalactosamine conjugated antisense oligonucleotides for targeted delivery to hepatocytes. *J. Med. Chem.*, **59**, 2718–2733.
24. Østergaard,M.E., Nichols,J., Dwight,T.A., Lima,W., Jung,M.E., Swayze,E.E. and Seth,P.P. (2017) Fluorinated nucleotide modifications modulate allele selectivity of SNP-targeting antisense oligonucleotides. *Mol. Ther. Nucleic Acids*, **7**, 20–30.
25. Nowotny,M., Gaidamakov,S.A., Ghirlando,R., Cerritelli,S.M., Crouch,R.J. and Yang,W. (2007) Structure of human RNase H1 complexed with an RNA/DNA hybrid: insight into HIV reverse transcription. *Mol. Cell*, **28**, 264–276.
26. Wan,W.B. and Seth,P.P. (2016) The medicinal chemistry of therapeutic oligonucleotides. *J. Med. Chem.*, **59**, 9645–9667.
27. Crooke,S.T., Witztum,J.L., Bennett,C.F. and Baker,B.F. (2018) RNA-targeted therapeutics. *Cell Metabolism*, **27**, 714–739.
28. Shen,X. and Corey,D.R. (2018) Chemistry, mechanism and clinical status of antisense oligonucleotides and duplex RNAs. *Nucleic Acids Res.*, **46**, 1584–1600.
29. Seth,P.P., Siwkowski,A., Allerson,C.R., Vasquez,G., Lee,S., Prakash,T.P., Wancewicz,E.V., Witchell,D. and Swayze,E.E. (2009) Short antisense oligonucleotides with novel 2′-4′ conformationaly restricted nucleoside analogues show improved potency without increased toxicity in animals. *J. Med. Chem.*, **52**, 10–13.
30. Straarup,E.M., Fisker,N., Hedtjarn,M., Lindholm,M.W., Rosenbohm,C., Aarup,V., Hansen,H.F., Orum,H., Hansen,J.B. and Koch,T. (2010) Short locked nucleic acid antisense oligonucleotides potently reduce apolipoprotein B mRNA and serum cholesterol in mice and non-human primates. *Nucleic Acids Res.*, **38**, 7100–7111.
31. Swayze,E.E., Siwkowski,A.M., Wancewicz,E.V., Migawa,M.T., Wyrzykiewicz,T.K., Hung,G., Monia,B.P. and Bennett,C.F. (2007) Antisense oligonucleotides containing locked nucleic acid improve potency but cause significant hepatotoxicity in animals. *Nucleic Acids Res.*, **35**, 687–700.
32. MacLeod,A.R. and Crooke,S.T. (2017) RNA therapeutics in oncology: advances, challenges, and future directions. *J. Clin. Pharmacol.*, **57**, S43–S59.
33. Hagedorn,P.H., Yakimov,V., Ottosen,S., Kammler,S., Nielsen,N.F., Høg,A.M., Hedtjärn,M., Meldgaard,M., Møller,M.R., Ørum,H. *et al.* (2013) Hepatotoxic potential of therapeutic oligonucleotides can be predicted from their sequence and modification pattern. *Nucleic Acid Ther.*, **23**, 302–310.
34. Burdick,A.D., Sciabola,S., Mantena,S.R., Hollingshead,B.D., Stanton,R., Warneke,J.A., Zeng,M., Martsen,E., Medvedev,A., Makarov,S.S. *et al.* (2014) Sequence motifs associated with hepatotoxicity of locked nucleic acid–modified antisense oligonucleotides. *Nucleic Acids Res.*, **42**, 4882–4891.
35. Kamola,P.J., Kitson,J.D.A., Turner,G., Maratou,K., Eriksson,S., Panjwani,A., Warnock,L.C., Douillard Guilloux,G.A., Moores,K., Koppe,E.L. *et al.* (2015) In silico and in vitro evaluation of exonic and intronic off-target effects form a critical element of therapeutic ASO gapmer optimization. *Nucleic Acids Res.*, **43**, 8638–8650.

36. Burel,S.A., Hart,C.E., Cauntay,P., Hsiao,J., Machemer,T., Katz,M., Watt,A., Bui,H.H., Younis,H., Sabripour,M. *et al.* (2016) Hepatotoxicity of high affinity gapmer antisense oligonucleotides is mediated by RNase H1 dependent promiscuous reduction of very long pre-mRNA transcripts. *Nucleic Acids Res.*, **44**, 2093–2109.
37. Kakiuchi-Kiyota,S., Koza-Taylor,P.H., Mantena,S.R., Nelms,L.F., Enayetallah,A.E., Hollingshead,B.D., Burdick,A.D., Reed,L.A., Warneke,J.A., Whiteley,L.O. *et al.* (2014) Comparison of hepatic transcription profiles of locked ribonucleic acid antisense oligonucleotides: evidence of distinct pathways contributing to non-target mediated toxicity in mice. *Toxicol. Sci.*, **138**, 234–248.
38. Kakiuchi-Kiyota,S., Whiteley,L.O., Ryan,A.M. and Mathialagan,N. (2015) Development of a Method for Profiling Protein Interactions with LNA-Modified Antisense Oligonucleotides Using Protein Microarrays. *Nucleic Acid Ther.*, **26**, 93–101.
39. Nowotny,M., Cerritelli,S.M., Ghirlando,R., Gaidamakov,S.A., Crouch,R.J. and Yang,W. (2008) Specific recognition of RNA/DNA hybrid and enhancement of human RNase H1 activity by HBD. *EMBO J.*, **27**, 1172–1181.
40. Cléry,A., Blatter,M. and Allain,F.H.T. (2008) RNA recognition motifs: boring? Not quite. *Curr. Opin. Struct. Biol.*, **18**, 290–298.
41. Messias,A.C. and Sattler,M. (2004) Structural basis of single-stranded RNA recognition. *Acc. Chem. Res.*, **37**, 279–287.
42. Kasuya,T. and Kugimiya,A. (2018) Role of computationally evaluated target specificity in the hepatotoxicity of gapmer antisense oligonucleotides. *Nucleic Acid Ther.*, **28**, 312–317.
43. Thomas,M.P., Liu,X., Whangbo,J., McCrossan,G., Sanborn,K.B., Basar,E., Walch,M. and Lieberman,J. (2015) Apoptosis triggers specific, rapid, and global mRNA decay with 3′ uridylated intermediates degraded by DIS3L2. *Cell Rep.*, **11**, 1079–1089.
44. Bailey,J.K., Shen,W., Liang,X-h. and Crooke,S.T. (2017) Nucleic acid binding proteins affect the subcellular distribution of phosphorothioate antisense oligonucleotides. *Nucleic Acids Res.*, **45**, 10649–10671.